ACS APPLIED MATERIALS & INTERFACES

Research Article

www.acsami.org

Marine Corrosion Protective Coatings of Hexagonal Boron Nitride Thin Films on Stainless Steel

Esam Husain,*[,†,‡] Tharangattu N. Narayanan,[†,§] Jose Jaime Taha-Tijerina,[†] Soumya Vinod,[†] Robert Vajtai,[†] and Pulickel M. Ajayan*[,†]

[†]Department of Mechanical Engineering & Materials Science, Rice University, Houston, Texas, United States

[‡]College of Technological Studies, Marine Engineering Technology Department, Kuwait

Supporting Information

ABSTRACT: Recently, two-dimensional, layered materials such as graphene and hexagonal boron nitride (h-BN) have been identified as interesting materials for a range of applications. Here, we demonstrate the corrosion prevention applications of h-BN in marine coatings. The performance of h-BN/polymer hybrid coatings, applied on stainless steel, were evaluated using electrochemical techniques in simulated seawater media [marine media]. h-BN/polymer coating shows an efficient corrosion protection with a low corrosion current density of 5.14×10^{-8} A/cm^2 and corrosion rate of 1.19×10^{-3} mm/year and it is attributed to the hydrophobic, inert and dielectric nature of boron nitride. The results indicated that the stainless steel with coatings exhibited improved corrosion resistance. Electrochemical impedance spectroscopy and potentiodynamic analysis were used to propose a mechanism for the increased corrosion resistance of h-BN coatings.

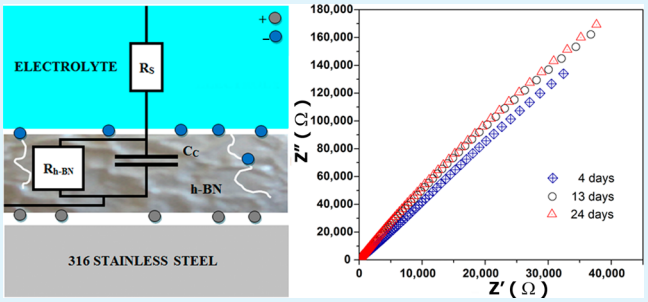

KEYWORDS: *marine corrosion, boron nitride coating, hydrophobic coating, corrosion protection, 2D nanomaterials, electrochemical analysis*

1. INTRODUCTION

Metallic corrosion leads to increased structural failures and huge economic losses in various industries. Different coating approaches have been studied in the past for corrosion protection, including ceramic coatings,[1−4] polymer coatings,[5−9] electrodeposition of nanocrystalline materials,[10−14] and self-assembled nanocoatings.[15−18] In addition to these techniques, a combination of above-mentioned methods, such as coatings using nanopaints, which contain nanomaterials in polymer paints, and multiphase nanomaterial-based coatings that can withstand high temperature, have also been tested.[19,20] Recent studies indicate that nanomaterials, because of their high surface area and high adhesion to substrates, provide effective corrosion resistance and can be used for protective coatings on various surfaces.[21,22]

Polymeric coatings and paints are widely used in industries for corrosion protection.[23−25] Multiphase coating consisting of three-layer TiO_2−Al_2O_3 nanocomposite films also showed good corrosion resistance when applied on 316L stainless steel (316LSS) by sol−gel process.[26] In the case of polymer paints, perfluorooctadecanoic acid (PFOA) PFS polymer paints exhibited enhanced corrosion protection. These experiments indicate that low-energy surfaces such as polished steels could be effectively protected using hydrophobic materials.[27−30] TiN-based alloy coatings on 316LSS, which is one of the most commonly used steels in industry, provided low corrosion current density and high charge transfer resistance.[31] Conducting polymer coatings, such as polyaniline (PANI)[32,33] and polypyrrole (PPy),[34−36] were also tested on stainless steel for improved corrosion resistance and increased electrical conductivity. However, the presence of porosity (pores and pinholes) in polymer coatings gives rise to corrosion on the substrates because of the attack of ions through the pores.

Hexagonal-boron nitride (h-BN) is a layered material consisting of two-dimensional (2D) atomically thin sheets of covalently bonded boron and nitrogen stacked together by weak van der Waals force. Recently, researchers have been able to exfoliate bulk h-BN materials in large quantities to obtain high surface area h-BN sheets using wet chemical approach and demonstrate its various applications.[37] h-BN is hydrophobic by nature and it can passivate surfaces effectively from water.[38] Recently, hydrophobic and atomically thin layered nanomaterials such as graphene[39−41] or h-BN[42,43] have proven their effectiveness in metallic corrosion resistance. In this study, we explore a method to increase the degree of corrosion protection by coating 316LSS with h-BN−polyvinyl alcohol (PVA) coating. Biofriendly polymer PVA is used as the binder to

Received: January 2, 2013
Accepted: April 25, 2013
Published: April 25, 2013

Table 1. Elemental Analysis of 316L stainless steel Using Energy-Dispersive Spectroscopy (EDS)

	atomic wt %										
	Cr	Ni	C	Mn	Cu	Mo	Si	S	b	other	Fe
316	18	14	0.08	2.0	0.75	3.0	1.0	0.03	0.045	N ~ 0.1	balance

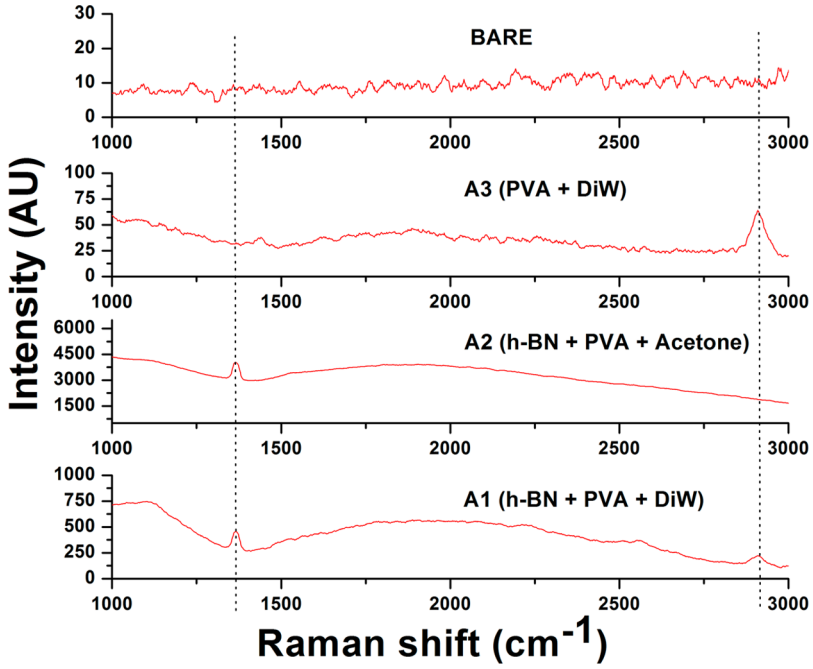

Figure 1. Raman spectra of various samples.

increase the adhesion of nano h-BN flakes (lower fraction of h-BN is also biofriendly and is already using in cosmetic materials) with the steel surface. Finally, with the electrochemical impedance spectrometry and potentiodynamic techniques, the pathways of corrosion reactions are elucidated for the h-BN coatings

2. EXPERIMENTAL PROCEDURE

2.1. Material. The corrosion/erosion studies were conducted on AISI 316LSS samples of area 1.98 cm^2 and thickness 5 mm. The elemental composition (in atomic wt %) is given in Table 1.

Simulated seawater was prepared and used as corrosive media. It was composed by adding 35 g of API aquarium salt (evaporated seawater natural salt) to a liter of deionized water (DiW) (3.5% of API salt). The pH of simulated seawater at room temperature (~300 K) matches with seawater from Gulf of Mexico (pH 6.5−7.0). Also, total dissolved solids (TDS) of simulated seawater is measured; 3 g/L. (TDS for DiW = 253 mg/L). Twenty-five mg of h-BN (procured from Sigma Aldrich (1 μm, 98%)) (FE-SEM image of the initial powder is shown in Supporting Information, Figure S1) is sonicated in 20 mL of PVA/water (acetone) for 6 h. The water assisted hydrolysis of h-BN occurred after this prolonged and temperature controlled (maintained room temperature ~23 °C) water bath sonication and the h-BN was found to be dispersed well in PVA/water. It was inferred that it is due to the fact that a huge part of h-BN is exfoliated in water because of the hydrolysis-assisted exfoliation.

2.2. Polishing Procedure. The ASTM G1-03 (2011)[44] procedure was followed for surface polishing of the steel samples. The 316LSS samples were ground with 300−1200 μm emery papers and polished with Al_2O_3 solution. The surfaces of the samples were finally ultrasonically cleaned using acetone, ethanol, and distilled water for 10 min, respectively.

2.3. Preparation of Coating. h-BN/PVA mixture are coated on steel samples using conventional spin coating and casting the samples for 24 h in an elevated temperature of 60 °C. Different h-BN/PVA samples and control samples named A1, A2, and A3 are prepared. Coating A1 contains h-BN/PVA dispersed in DI water (100 mg of h-BN, 25 mg of PVA, 20 mL of DI water). A2 contains h-BN/PVA dispersed in acetone (100 mg of h-BN, 25 mg of PVA, 20 mL of acetone). A3 contains controlled sample with PVA in water (25 mg of PVA in 20 mL of DI water). The thickness of the coating was studied using cross sectional SEM (A1 sample average ~9.33 μm) (shown in the Supporting Information, Figure S2).

2.4. Surface Characterization. Surface topography and elemental analysis of the coating was characterized by SEM and Raman spectroscopy and adhesion measurement was conducted using Instron impact equipment. Zeta potential studies were carried out using Malvern Zen 3600 Zetasizer (Zetasizer Nano) instrument. A1 coating suspension was subjected to zeta potential studies to identify the stability and was found to be highly stable, with a zeta potential value of approximately −30 mV.

2.5. Electrochemical Measurements. The measurements of polarization curves and electrochemical impedance spectroscopy (EIS) are carried out in a three electrode cell in simulated seawater media using Autolab PGSTAT 30 electrochemical measurement system (shown in the Supporting Information, Figure S3). Samples A1, A2, and A3 were used as working electrode and the test cell included a platinum auxiliary electrode and a Ag/AgCl reference electrode. Polarization tests were carried out in the scan range between −300 to 1000 mV at a scan rate of 0.2 mV/s. The impedance measurements were carried out at the open circuit potential (OCP) with amplitude of 10 mV in the frequency range between 100 kHz and 10 mHz. All samples were kept in solution for 1 h to reach the open-circuit potential.

3. RESULTS AND DISCUSSION

3.1. Surface Characterization. Raman studies were conducted on bare, A1, A2, and A3 steel samples using 514.5

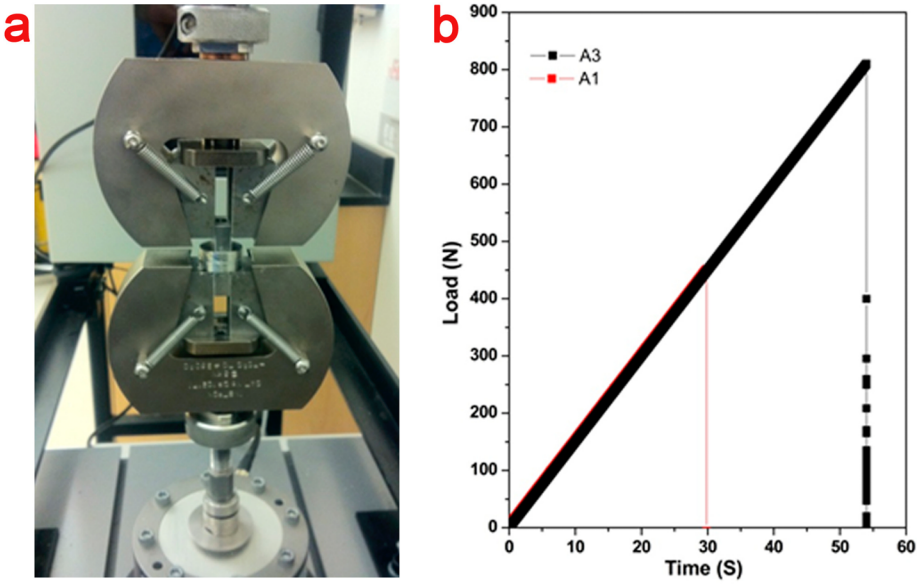

Figure 2. (a) Adhesion test equipment; (b) surface adhesion test on A1 and A3.

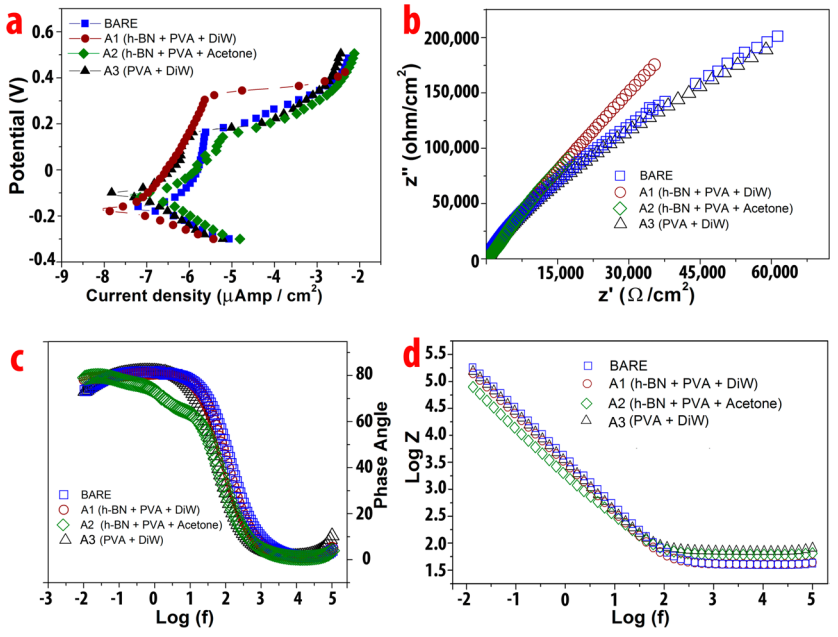

Figure 3. (a) Polarization curve after 1 h; (b) Nyquist plot; (c) Bode plots for phase angle vs frequency; and (d) impedance vs frequency for different samples after immersion in simulated seawater for 30 days.

nm laser excitation. Figure 1 shows the Raman spectrum of different samples. Bare steel sample shows no Raman modes, whereas A3 shows only that of PVA.

Both A1 and A2 show the signature of h-BN E_{2g} mode at ~1369 cm^{-1}, indicating the presence of h-BN in the coatings. The surface adhesion of the polymer nanocomposite to the steel surface is conducted using Instron adhesion equipment, (shown in Figure 2a). Standards ISO 4624 and ASTM D4145[45] were followed for the adhesion tests. One sample is coated with slow curing resin and the other with A1 or A3 films. Both the samples were then held together using a clamp for 1 day to dry. The adhesion results show that (Figure 2b) both A1 and A3 have good adhesion to the surface with a film detachment value of 420N for A1, whereas that for A3 is 820N. PVA could not well disperse in acetone for making A2, and the adhesion tests were also failed in the case of A2. The comparatively lower adhesion of A1 may be due to the presence of h-BN nano flakes in the PVA polymer matrix.

3.2. Polarization Curves. Figure 3 shows the potentiodynamic and electrochemical impedance studies for bare, A1, A2, and A3 samples when exposed to simulated seawater media at room temperature. Polarization curve (Figure 3a) (after 1 h) show noble E_{pit} value and lower current densities in the anodic region for sample A1, which implies a higher corrosion resistance. A1 introduces a shift in the corrosion potential to more noble value compared with A2 and A3 coatings, combined with an increase in the passive range, for a scan potential range from −0.18 V to the breakdown potential (E_{pit}) at +0.320 V. A2 and A3 polarization curves showed similar E_{pit} values of ~ +0.18 V but different current densities. The larger

dx.doi.org/10.1021/am400016y | ACS Appl. Mater. Interfaces 2013, 5, 4129−4135

diameter curve in the Nyquist plot (Figure 3b) for sample A1 shows higher Z'', which means the coating is more capacitive, providing more protection against corrosion. The phase angle for A1, which is higher than 80° (Figure 3c), and the high value of impedance (in Figure 3d) indicates that the coating is more capacitive than resistive. The Bode plot did not show much variation among different samples, and longer immersion times are required to see the difference.

Scanning electron microscopy (SEM) along with energy-dispersive spectroscopy (EDS) are used to investigate the effect of simulated seawater media for long immersion times (30 days) on h-BN-coated 316L stainless steel and other samples. Images a and b in Figure 4 shows typical h-BN coating (A1)

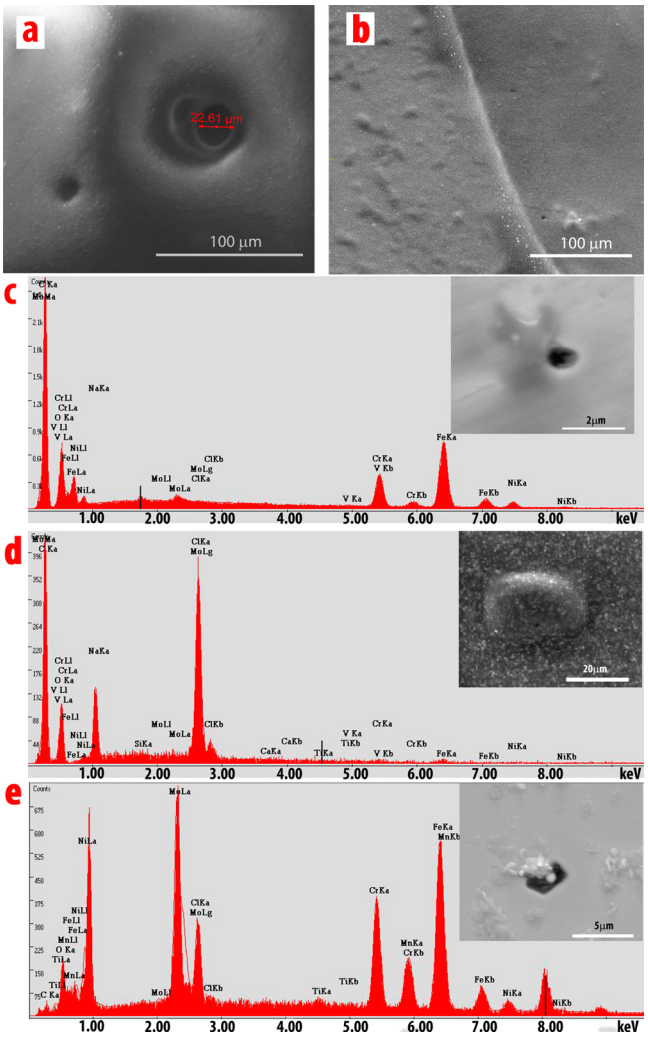

Figure 4. (a) SEM of a pit in A1, (b) SEM of A1 after polarization in simulated seawater showing blisters development, SEM of pit formed and EDS spectra from the pit for, (c) A1, (d) A2, and (e) A3 samples.

with various pinholes defects and coating blisters after 30 days of immersion, which can be due to the water ions permeation through the coating, which could be caused by crevice or localized corrosion exhibited under the sealing rubber "O"-ring. EDS analysis was performed on the corrosion pit of A1 (corresponding SEM where the electron beam is focused on one of the pinholes is shown as inset) and revealed the presence of iron (Fe) and oxygen (O_2), similar to A2 and A3 coatings, other than the presence of elements like C, Mo, Ni, and Cr (those elements are part of the stainless steel). Bigger pits and blisters were observed from SEM images of A2 and A3 too, taken after the polarization studies (Figure 4d, e). Moreover, in A2 and A3, one could see large amount of Cl content, possibly due to the larger penetration of seawater media and deposition of salt in the pits, whereas A1 still acts as a hydrophobic coating because of the presence of h-BN.

After anodic polarization studies, no corrosion products are found on A1 coating surface and only some shrinkage was observed. In relation to electrochemical polarization, these images validate the measurements, hence as soon as the simulated seawater media penetrates through the layers of coating and reaches the substrate, an electrochemical reaction takes place, for example in the case of A1 (E_{pit} = +0.320 V) causing a sudden increase of current density.[46]

Table 2 depicts the corrosion properties of the specimens obtained from the polarization test (after curve fitting Figure

Table 2. Tafel Parameters for Different Working Electrodes from Polarization Curves after 1 h

coating type	E_{corr} (V)	I_{corr} (A/cm^2)	corr. rate (mm/year)
bare	−0.165	1.07×10^{-7}	2.51×10^{-3}
A1	−0.236	5.14×10^{-8}	1.19×10^{-3}
A2	−0.112	5.90×10^{-8}	1.37×10^{-3}
A3	−0.125	1.04×10^{-7}	2.42×10^{-3}

3a). The corrosion current (I_{corr}) and corrosion potential (E_{corr}) were determined from the polarization curve using the Tafel extrapolation method. The corresponding current and potential at the point of intersection of the extrapolated anodic and cathodic polarization curves gives I_{corr} and E_{corr}, respectively. From the corrosion current density, the corrosion rate is calculated using the following equation[47]

$$CR = (0.00327 I_{corr} W)/(nD) \quad (1)$$

Where W is the atomic weight of steel (56.3 g/mol), n is the number of electrons transferred in the corrosion reaction (n = 2), and D is the density of steel (7.89 g/cm^3). It can be seen from Table 2 that the corrosion current and corrosion rate for sample A1 is lower compared to other samples, which means increased resistance to corrosion.

Metastable pitting on stainless steels was observed at potentials below the pitting potential, or above the pitting potential before the beginning of stable pitting.[48] This means that the rate of growth of individual corrosion pit is controlled by diffusion of the dissolving metal cations from the pit interior, the surface of which is saturated with the metal chloride. This process is independent of electrode potential. Analysis of the diffusion yields a critical value of the product of the pit radius and its dissolution current density (termed the "pit stability product"), below which the pit is metastable and may repassivate, and above which the pit is stable.[48−50] The anodic current densities show A1 as the most corrosion resistant among the samples. It is reported that molybdenum changes the anodic dissolution kinetics of the active pit surface.[31,51] Hydrophobic h-BN films tend to increase stainless steel anodic potential, and hence works as species and ionic exchange retardant.

This means that h-BN coatings can effectively inhibit the inward penetration of ions, such as $Cl^-$and Fe^-, the observed decrease in current density resulting in higher corrosion resistance. Moreover, after the anodic polarization, optical

and elemental analysis showed that localized pitting corrosion is observed on A2 and A3 samples, which resulted in small pits and blisters of different sizes (shown in the Supporting Information, Figure S4).This indicates a preferential localized attack, occurring after the electric potential exceeded the breakdown potential. This localized attack results in delaminating and lifting of the coating from the substrate, possibly because of the hydrolysis reactions happening at the interface.

3.3. EIS Spectra Analysis. Figure 5 shows the results of the log impedance magnitude spectra of A1 under simulated seawater environment after 30 days' test at room temperature for various periods. This result validate previous impedance spectra in Figure 3b, as A1 coating become more capacitive with time, this due to good ionic exchange of h-BN barrier exhibit with PVA polymer binder in DiW, which stayed intact to the stainless steel. This consequently lead to the low corrosion rate, but A2 and A3 coatings showed slow degradation as immersion period increases.

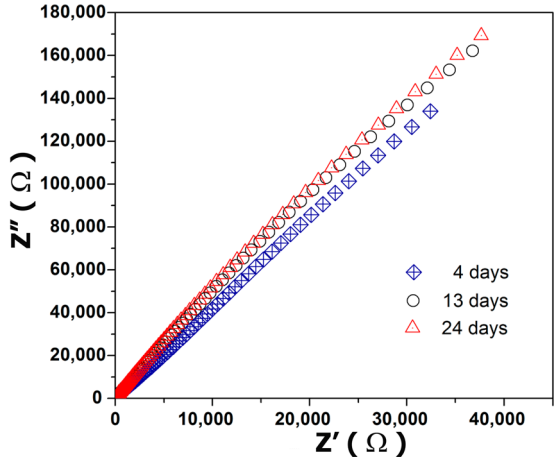

Figure 5. A1 coating impedance at different immersion time.

A model is put forwarded on the basis of polarization data, impedance spectroscopy results and optical pitting observation, to explain the observed electrochemical behavior of h-BN-coated steel surfaces. The following mechanisms (Figure 6) are suggested for the impedance circuitry in A1 and A2/A3. The equivalent circuit was obtained by fitting the EIS data to the circuit model in the Autolab FRA software.

R_s is the solution resistance, $R_{h\text{-}BN}$ is the coating resistance (for A3, coating resistance $R_{h\text{-}BN}$ is coming from the PVA) and C_c is the capacitance of the coating. R_{ct} and C_{dl} are the charge transfer resistance and double-layer capacitance, respectively. Coatings that are intact have only one time constant but for imperfect coatings, the underlying metal comes in contact with the solution, and hence R_{ct} and C_{dl} of the metal surface also need to be included in the equivalent circuit. This explains the circuit with one time constant for A1 and two time constants for A2 and A3 coatings.

Experimental data were compared with the model and the results are shown in Table 3, showed good coherence between the fit to the measured data, in spite of the approximations made. The impedance elements of A2 and A3 coatings suggests that the electrochemical processes might be controlled by the active species diffusing to the metal surface or corrosion products diffusing away from the metal surface through the coating film, whereas the A1 coating remains a purely capacitive one.

Table 3. Electrical Equivalent Circuit Parameters for Different Samples[a]

coating type	C_C (μF/cm^2)	$R_{h\text{-}BN}$ (KΩ/cm^2)	R_S (Ω/cm^2)	R_{ct} (Ω/cm^2)	C_{dl} (μF/cm^2)
bare	70.4	10	38	44 × 10^4	44
A1: h-BN+ PVA + DiW	75	210	38		
A2: h-BN + PVA + acetone	60	2	61	31.7	330
A3: PVA + DiW	56.7	206	70.9	54.9	10

[a]Note: Parameters were calculated by curve fitting using AutoLab frequency response analyzer (shown in the Supporting Information, Figure S5).

In general, when the electrolyte permeates the polymer film, coating capacitance (C_c) may be observed to increase, which is related to an increase of dielectric constant ε, due to the increased water absorption. The coating resistance, ($R_{h\text{-}BN}$), is observed to decrease with exposure duration as existing pores are permeated with electrolyte, increasing the ionic conductivity in the coating. The solution then begins to contact the metal/coating interface. Corrosion may occur depend on the pH, conductivity of the film and concentration of cations and anions in simulated seawater media. The presence of ions in the film

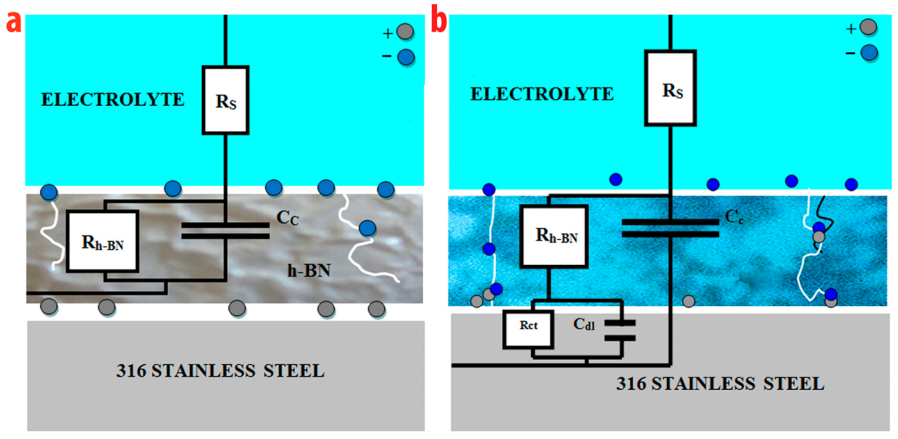

Figure 6. Electrochemical corrosion models for (a) A1 and (b) A2/A3 coatings.

and on the metal substrate will give rise to a loss in coating electrical resistance and a rise in substrate corrosion, accounted by a decrease in the faradic resistance. Overall, most coatings behaved as a purely capacitive dielectric with a slope of −1 and a phase angle of −85°, a pure resistor is shown as a horizontal line for the log impedance with angle of ∼0°.

4. CONCLUSIONS

h-BN-based polymer paint is successfully tested for its metallic corrosion resistance under a simulated seawater media. The electrochemical studies indicated that h-BN films can serve as an excellent corrosion-inhibiting coatings and developed quantitative models that describe the corrosion protection mechanism. The data show minor crevice corrosion occurs with localized pits between metal and coating interface particularly for A2 and A3 coatings. Finally, we demonstrate that combination of simple electrochemical techniques can be effectively used to characterize the h-BN protective coatings.

■ ASSOCIATED CONTENT

Ⓢ Supporting Information

Details of electrochemical corrosion cell setup, SEM analysis, and curve fittings for EIS data. These materials is available free of charge via the Internet at http://pubs.acs.org

■ AUTHOR INFORMATION

Corresponding Author

*E-mail: e.matouq@paaet.edu.kw (E.H.), ajayan@rice.edu (P.M.A.).

Present Address

[§]CSIR - Central Electrochemical Research Institute, Karaikudi, Tamilnadu, India.

Notes

The authors declare no competing financial interest.

■ ACKNOWLEDGMENTS

E.H. acknowledges Dr. A. Al-Nafisi, PAAET General Director, for sabbatical leave financial support, and Dr Adel. Husain, KISR, for his academic analytical support. P.M.A., N.T.N., R.V., and J.J.T.-T. acknowledge funding from the U.S. Army Research Office MURI Grant W911NF- 11-1-0362, the U.S. Office of Naval Research MURI Grant N000014-09-1-1066 on novel free-Standing 2D crystalline materials focusing on atomic layers of nitrides, oxides, and sulfides. J.J.T.-T. acknowledges the support from PGE and CONACYT (213780). S.V. and R.V. acknowledge the support provided by the Department of Energy (DOE) Grant DE-SC0001479.

■ REFERENCES

(1) Jensen, H.; Sorensen, G. *Surf. Coat. Technol.* **1996**, *84*, 500−505.
(2) Droniou, P.; Fristad, W. E.; Liang; Li., J. *Coatings* **2005**, *38*, 237−239.
(3) Shen, G. X.; Chen, Y. C.; Lin, L.; Lin, C. J.; Scantlebury, D. *Electrochim. Acta* **2005**, *50*, 5083−5089.
(4) Euler, F.; Jakob, C.; Romanus, H.; Spiess, L.; Wielage, B.; Lampke, T.; Steinha, S. *Electrochim. Acta* **2003**, *48*, 3063−3070.
(5) Rout, T. K.; Jha, G.; Singh, A. K.; Bandyopadhyay, N.; Mohanty, O. N. *Surf. Coat. Technol.* **2003**, *167*, 16−24.
(6) Wessling, B.; Posdorfer, J. *Synth. Met.* **1999**, *102*, 1400−1401.
(7) Garcia, B.; Lamzoudi, A.; Pillier, F.; Le, H. N. T.; Deslouis, C. *J. Electrochem. Soc.* **2002**, *149*, 52−60.
(8) Yeh, J. M.; Chin, C. P. *J. Appl. Polym. Sci.* **2003**, *88*, 1072−1078.
(9) Kendig, M.; Hon, M.; Warren, L. *Prog. Org. Coat.* **2003**, *47*, 183−189.
(10) Thorpe, S. J.; Ramaswami, B.; Aust, K. T. *J. Electrochem. Soc.* **1988**, *135*, 2162−2170.
(11) Bragagnolo, P.; Waseda, Y.; Palumbo, G.; Aust, K. T. *MRS Symp.* **1989**, *4*, 469−474.
(12) Zeiger, W.; Schneider, M.; Scharnwber, D.; Worch, H. *Nanostruct. Mater.* **1995**, *6*, 1013−1016.
(13) Barbucci, A.; Farne, G.; Mattaezzi, P.; Riccieri, R.; Cereisola, G. *Corros. Sci.* **1999**, *41*, 463−475.
(14) Alves, H.; Ferreira, M. G. S.; Koster, U. *Corros. Sci.* **2003**, *45*, 1833−1845.
(15) Zheludkevich, M. L.; Miranda Salvado, I. M.; Ferreira, M. G. S. *J. Mater. Chem.* **2005**, *15*, 5099−5111.
(16) Zheludkevich, M. L.; Serra, R.; Montemor, M. F.; Miranda Salvado, I. M.; Ferreira, M. G. S. *Surf. Coat. Technol.* **2006**, *200*, 3084−3094.
(17) Zheludkevich, M. L.; Serra, R.; Montemor, M. F.; Yasakau, K. A.; Miranda Salvado, I. M.; Ferreira, M. G. S. *Electrochim. Acta* **2005**, *51*, 208−217.
(18) Voevodin, N. N.; Kurdziel, J. W.; Mantz, R. *Surf. Coat. Technol.* **2006**, *201*, 1080−1084.
(19) Sobolov, K.; Gutierrez, M. F. *Am. Ceram. Soc. Bull.* **2005**, *84*, 14−17.
(20) Baer, D. R.; Burrows, P. E.; El-Azab, A. A. *Prog. Org. Coat.* **2003**, *47*, 342−356.
(21) Voevodin, N.; Balbyshev, V. N.; Khobaib, M.; Donley, M. S. *Prog. Org. Coat.* **2003**, *47*, 416−423.
(22) Bjerklie, S. *Met. Finish.* **2005**, *103*, 46−47.
(23) Zanda, R. Z.; Verbekenb, K.; Adriaensa, A. *Prog. Org. Coat.* **2011**, *72*, 709−715.
(24) Mansfeld, F. *J. Appl. Electrochem.* **1995**, *25*, 187−202.
(25) Lee, W. G.; Jang, H. *Bull. Korean Chem. Soc.* **2012**, *33*, 1177−1182.
(26) Vaghari, H.; Sadeghian, Z.; Shahmiri, M. *Surf. Coat. Technol.* **2011**, *205*, 5414−5421.
(27) Kruszewski, K. M.; Gawalt, E. S. *Langmuir* **2011**, *27*, 8120−8125.
(28) Hasannejad, H.; ShahrabI, T.; Rouhaghdam, A. S.; Aliofkhazraei, M. *Mater. Sci. Technol.* **2008**, *24*, 715−717.
(29) Yang, Q.; Cai, F.; Zhao, L. R.; Huang, X. *Surf. Coat. Technol.* **2008**, *203*, 606−609.
(30) Gonzalez, M. B.; Saidman, S. B. *Corros. Sci.* **2011**, *53*, 276−282.
(31) Ilevbare, G. O.; Burstein, G. T. *Corros. Sci.* **2001**, *43*, 485−513.
(32) Nam, N. D.; Kim, J. G.; Lee, Y. J.; Son, Y. K. *Corros. Sci.* **2009**, *51*, 3007−3013.
(33) Joseph, S.; McClure, J. C.; Chianelli, R.; Pich, P.; Sebastian, P. J. *Int. J. Hydrogen Energy* **2005**, *30*, 1339−1344.
(34) Wang, Y.; Northwood, D. O. *J. Power Sources* **2006**, *163*, 500−508.
(35) Le, D. P.; Yoo, Y. H.; Kim, J. G.; Cho, S. M.; Son, Y. K. *Corros. Sci.* **2009**, *51*, 330−338.
(36) Nam, N. D.; Jo, D. S.; Kim, J. G.; Yoon, D. H. *Thin Solid Films* **2011**, *519*, 6787−6791.
(37) Taha-Tijerina, J.; Narayanan, T. N.; Gao, G.; Rohde, M.; Tsentalovich, D.; Pasquali, M.; Ajayan, P. M. *ACS Nano* **2012**, *6*, 1214−1220.
(38) Pakdel, A.; Zhi, C.; Bando, Y.; Nakayama, T.; Golberg, D. *ACS Nano* **2011**, *5*, 6507−6515.
(39) Li, G. X.; Liu, Y.; Wang, B.; Song, X. M.; Li, E.; Yan, H. *Appl. Surf. Sci.* **2008**, *254*, 5299.
(40) Chen, S.; Brown, L.; Levendorf, M.; Cai, W.; Ju, S-Y; Edgeworth, J.; Li, X.; Magnuson, C. W.; Velamakanni, A.; Piner, R. D.; Kang, J.; Park, J.; Ruoff, R. S. *ACS Nano* **2012**, *5*, 1321−1327.
(41) Singh Raman, R. K.; Chakraborty Banerjee, P.; Lobo, D. E.; Gullapalli, H.; Sumandasa, M.; Kumar, A.; Choudhary, L.; Tkacz, R.; Ajayan, P. M.; Majumder, M. *Carbon* **2012**, *50*, 4040−4045.
(42) Marchetti, F.; Fedrizzi, L.; Giacomozzi, F.; Guzman, L.; Borgese, A. *Mater. Sci. Eng., A* **1985**, *69*, 289−295.

(43) Dikici, B.; Ozdemir, I. *Anti-Corros. Method. Mater.* **2012**, *59*, 246−254.
(44) *ASTM G1-03(2011) Standard Practice for Preparing, Cleaning, and Evaluating Corrosion Test Specimens*; ASTM International: West Conshohocken, PA, 2011.
(45) (a) *ASTM D4145-10 Standard Test Method for Coating Flexibility of Prepainted Sheet*; ASTM International: West Conshohocken, PA, 2010. (b) *ISO 4624 - Paints, Varnishes and Plastics, Pull-off Test for Adhesion*; International Organization for Standardization: Geneva, Switzerland, 2012.
(46) Carbajal-de la, Torre; Espinosa-Medina, M. A.; Martinez-Villafane, A.; Gonzalez-Rodriguez, J. G.; Castano, V. M. *Open Corros. J.* **2009**, *2*, 197−203.
(47) Hamah-Ali, B.; Ali, B. S.; Yusoff, R.; Aroua, M. K. *Int. J. Electrochem. Sci.* **2011**, *6*, 181−198.
(48) Stewart, J.; Williams, D. E. *Corros. Sci.* **1992**, *33*, 457−463.
(49) Eichler, J.; Lesniak, C. *J. Eur. Ceram. Soc.* **2008**, *28*, 1105−11109.
(50) Lipp, A.; Schwetz, K. A.; Hunold, K. *J. Eur. Ceram. Soc.* **1989**, *5*, 3−9.
(51) Hara, N.; Hirabayashi, K.; Sugawara, Y.; Muto, I. *Int. J. Corros.* **2012**, *482730*, 6.